Journal of Contaminant Hydrology 197 (2017) 29–38

Contents lists available at ScienceDirect

Journal of Contaminant Hydrology

journal homepage: www.elsevier.com/locate/jconhyd

Investigation of hexavalent chromium sorption in serpentine sediments

Thanasis Mpouras [a,*], Maria Chrysochoou [b], Dimitris Dermatas [a]

[a] School of Civil Engineering, Department of Water Resources and Environmental Engineering, National Technical University of Athens, Iroon Polytechniou 9, 157 80 Zografou, Greece
[b] Department of Civil and Environmental Engineering, University of Connecticut, Storrs, CT, USA

ARTICLE INFO

Article history:
Received 25 June 2016
Received in revised form 2 November 2016
Accepted 25 December 2016
Available online 5 January 2017

Keywords:
Hexavalent chromium
Serpentine sediment
Adsorption
Reduction

ABSTRACT

In this study the removal of hexavalent chromium (Cr^{6+}) by serpentine sediments was investigated in order to delineate Cr^{6+} sorption behavior in aquifers with ultramafic geologic background. Batch experiments were conducted in order to determine the influence of several parameters on Cr^{6+} removal, including the pH of the sediment solution, mineralogy, sediment's particle size and Cr^{6+} initial concentration. The results showed that Cr^{6+} removal was due to both adsorption and reduction phenomena. Reduction was attributed to the presence of a magnetic fraction in the sediment, mostly related to magnetite, which contributed almost 50% of the total removal in the pH range 3–7. Adsorption behavior was dominated by the finer sediment fraction ($d < 0.075$ mm). The amount of Cr^{6+} adsorbed was constant in the pH range 3–7, while it decreased sharply in the range 7–8.5. Cr^{6+} adsorption was found to increase and decrease proportionally with increasing initial Cr^{6+} concentration of and particle size, respectively. The linear Langmuir and Freundlich adsorption isotherms were used to describe the experimental data, with Freundlich providing a better fit to determine distribution factors for transport modeling.

1. Introduction

Groundwater contamination by heavy metals is one of the most important environmental problems. Chromium (Cr) is a heavy metal that occurs in several oxidation states, but only two prevail in the geoenvironment, trivalent (Cr^{3+}) and hexavalent (Cr^{6+}) (Richard and Bourg, 1991). High concentrations of Cr^{6+} in soil and groundwater are commonly attributed to anthropogenic activities. However, recent studies have shown that the occurrence of Cr^{6+} can also be of geogenic origin (Becquer et al., 2003; Bonifacio et al., 1997; Caillaud et al., 2009; Cheng et al., 2011; D'Amico et al., 2008; Dermatas et al., 2015; Garnier et al., 2006; Gonzalez et al., 2005; Hseu, 2006; Oze et al., 2007). Ultramafic rocks, and specifically serpentinites, are commonly associated with high concentrations of Cr^{3+}, up to 60,000 mg/kg. These rocks are also characterized by significant concentrations of magnesium (Mg), nickel (Ni) and cobalt (Co) (Oze et al., 2004). Although Cr^{3+} is the predominant state in most minerals observed in these rocks, groundwater interacting with such geological background can exhibit high Cr^{6+} concentrations, exceeding the limit of 50 μg/L proposed by the World Health Organization (WHO) (1993). This is due to weathering processes that make Cr^{3+} available for oxidation by high-valence manganese oxides (e.g., δ-MnO_2), which is subsequently released as highly mobile Cr^{6+} in groundwater (Oze et al., 2007).

In aqueous media Cr^{6+} occurs in anionic forms, namely chromate (CrO_4^{2-}), hydrogen chromate ($HCrO_4^-$) and dichromate ($Cr_2O_7^{2-}$) depending mainly on the pH values of the media. In the case of groundwater, since pH values range between 6 and 9, Cr^{6+} exists mainly as chromates. Several studies have reported high correlation between Cr^{6+} and total Cr (Cr_{tot}) concentrations in serpentine aquifers, thus effectively confirming the fact that it is the only form that can be transported with groundwater (Dermatas et al., 2015; Fantoni et al., 2002; Margiotta et al., 2012). Reduction and adsorption-desorption are the main processes that retard Cr^{6+} transport (Economou-Eliopoulos et al., 2014).

Cr^{6+} reduction in natural environments is facilitated by ferrous iron, sulfides and organic matter (Fendorf, 1995), while bacterially mediated reduction is also possible (Oliver et al., 2003; Xiao et al., 2014). Metal (hydr)oxides, especially Fe- and Al-oxides, are the primary minerals that control adsorption of Cr^{6+} in soils (Ajouyed et al., 2010; Álvarez-Ayuso et al., 2007; Fernández-Pazos et al., 2013; Otero et al., 2015; Zachara et al., 1987). Adsorption is a pH dependent process, controlled by the point of zero charge (PZC) of the mineral surface. At pH < PZC, surfaces are positively charged and Cr^{6+} adsorption increases with decreasing pH. For pH values greater than the PZC adsorption is minimized due to electrostatic repulsions between the chromate anions and the negatively charged surface (Sposito, 1989). Due to their relatively high PZC, iron (hydr)oxides such as goethite ($Fe^{3+}OOH$) (Abdel-Samad and Watson, 1997; Ajouyed et al., 2010; Mishra, 2012), ferrihydrite ($(Fe^{3+})_2O_3 \cdot 0.5H_2O$) (Tzou et al., 2003) and hematite

Abbreviations: BET, Brunauer–Emmett–Teller; PZC, point of zero charge; SEM, scanning electron microscopy; SSA, specific surface area; WHO, World Health Organization; XRD, X-ray diffraction; XRF, X-ray fluorescence.

* Corresponding author.
E-mail address: th.mpouras@gmail.com (T. Mpouras).

http://dx.doi.org/10.1016/j.jconhyd.2016.12.009
0169-7722/

($(Fe^{3+})_2O_3$) (Adegoke and Adekola, 2012; Ajouyed et al., 2010; Hejri et al., 2015) are known adsorbents for anions including Cr^{6+}. Magnetite ($Fe^{2+}(Fe^{3+})_2O_4$) is also a common soil mineral able to adsorb and subsequently reduce Cr^{6+} on its surface (Peterson et al., 1996; Jung et al., 2007; Choi et al., 2008).

While several studies have reported the presence of iron (hydr)oxides in serpentine soils and sediments (Becquer et al., 2003; Bonifacio et al., 1997; Caillaud et al., 2004; Fandeur et al., 2009; Kelepertzis et al., 2013), there is no information with regard to Cr^{6+} sorption behavior in aquifers with ultramafic (serpentine) geologic background. Given the importance of sorption for transport, such knowledge is necessary in order to evaluate mobility of Cr^{6+} in serpentine aquifers. Accordingly, the aim of the present study is to investigate the processes that affect Cr^{6+} removal in serpentine sediments from an ultramafic region in Greece, and study these processes as a function of pH, mineralogy, sediment's particle size and initial concentration of Cr^{6+}. In addition, Langmuir and Freundlich isotherms are fitted in order to extract the necessary distribution factors for transport modeling. This work is the first step in developing a more general framework to quantify and model the adsorption of Cr^{6+} on serpentine soils and sediments.

2. Materials and methods

2.1. Sediment sampling and analysis

The sediment samples were obtained from a sampling program conducted in the Vergina area in northern Greece (Dermatas et al., 2015). This area is characterized by an ultramafic geological background (Latsoudas and Sonis, 1991; Papanikolaou, 2009). During drilling, continuous core sampling (every 20–50 cm) took place down to 94 m depth. Four different aquifers were encountered at various depths (41–49 m, 54–60 m, 74–86 m and 91–94 m). Details of the sampling campaign and the characterization results are provided by Dermatas et al. (2015). Sediment samples for the present study were collected from the first aquifer at 41–49 m. The grain size distribution curve was obtained according to the ASTM D 422-72 method. Afterwards, the fraction smaller than 0.5 mm was utilized to conduct all adsorption experiments, allowing improved sample homogenization for further sub-sampling. Given that adsorption is typically dominated by smaller particle sizes, exclusion of larger particles should have minimal impact on the quantitative results and Kd values.

Sediment characterization included pH measurements according to method SW-846 (US EPA 9045C). Elemental analysis was carried out using X-ray fluorescence spectrometry (XRF) (Spectro Xepos). Sample preparation involved drying at 103 °C for 24 h and crushing to −100 μm. The total organic carbon (TOC) was measured using the Walkley-Black method. The total Cr^{6+} concentration naturally occurring in the samples was determined using EPA methods 3060A (alkaline digestion) followed by 7196A (diphenylcarbazide). The total specific surface area was determined by the N_2/BET adsorption method.

The mineralogical composition of the −0.5 mm fraction was assessed by powder X-ray diffraction (XRD), using a D8 Bruker Focus X-ray diffractometer. XRD patterns were collected between 5° and 65° with a 0.02° step size. Data were processed using the Jade software (Materials Data, Inc.) with reference to the International Center for Diffraction Data database. Quantitative XRD analysis was performed using the Whole Pattern Fitting method of Jade, suing structural data from the American Mineralogist Crystal Structure database. In addition, a scanning electron microscopy (SEM) analysis was performed using a JEOL JSM 5600 microscope equipped with an energy dispersive spectrometer (EDS) (Oxford ISIS 300).

2.2. Batch experiments

Batch experiments were performed for investigating the effect of a) pH, b) mineralogy, c) sediment's particle size and d) Cr^{6+} initial concentration, on Cr^{6+} adsorption. Sediment samples were sterilized prior to the experiments in order to prevent microbial reduction of Cr^{6+}. It is expected that the fine sediment fraction determines the adsorption process in the aquifers and since the finer the fraction, the greater the adsorption effects, sediment with grain size <0.5 mm was used in all the series of experiments at a concentration of 20 g/L. The effect of pH on adsorption was tested using initial Cr^{6+} concentration equal to 250 μg/L. This concentration was chosen as the upper limit of Cr^{6+} concentration in an aquifer with ophiolitic background and low contribution of anthropogenic activities. Specifically, agricultural activities taking place in the Vergina region may increase the mobilization of geogenic Cr^{6+} due to the addition of ammonium and phosphate based fertilizers (Becquer et al., 2003; Mills et al., 2011). The experiments were carried out at room temperature (25 °C), in a 0.01 M NaCl solution, in the pH range from 3 to 9. The pH adjustment was performed using HCl/NaOH solutions of 1 M. Erlenmeyer flasks containing 50 mL of the suspension were placed in an orbital shaker at 200 rpm for 24 h. For Cr^{6+} determination sediment solutions were filtered using 0.45 μm pore filters and Cr^{6+} was then determined using EPA method 7196A. The tests were carried out in triplicates.

The removal of Cr^{6+} was determined by the difference between the initial and the final concentration in the equilibrium solution of Cr^{6+}, according the following equation.

$$\%\text{removal} = \frac{C_0 - C_f}{C_0} \cdot 100 \quad (1)$$

where, C_0 (μg/L) is the initial concentration of Cr^{6+} and C_f (μg/L) the final concentration of Cr^{6+} in the equilibrium solution.

After removal of the supernatant and filtration, the recovered sediment was added again to a 0.01 M NaCl solution and the pH was raised to 11. The suspension was shaken for another 24 h to facilitate complete desorption of Cr^{6+} into solution. The recovered Cr^{6+} in this solution was measured using the same filtration and analysis process. Thus, the following concentrations of Cr^{6+} may be defined at every pH:

- Cr^{6+} removed: Cr^{6+} added (250 μg/L) – Cr^{6+} remaining in solution at the given pH
- Cr^{6+} adsorbed: Cr^{6+} released in solution at pH 11 - Cr^{6+} naturally occurring in sediment
- Cr^{6+} reduced: Cr^{6+} removed – Cr^{6+} adsorbed

2.2.1. Effect of mineralogy

In the pH edge experiments, the presence of black grains with magnetic properties was observed upon addition of the sediment in the NaCl solution. This magnetic fraction was easily removed using a magnetic bar. Three series of experiments were carried using the initial sediment sample (bulk sediment), the residual soil fraction after the removal of the magnetic fraction (non-magnetic fraction) and the isolated magnetic fraction.

2.2.2. Effect of particle size

The effect of particle size was tested using the non-magnetic sediment fraction. The non-magnetic sample with grain size <0.5 mm was further sieved in order to obtain the three following fractions: a) 0.5 mm < d < 0.25 mm, b) 0.25 mm < d < 0.075 mm, c) d < 0.075 mm. Sampling from the obtained fractions was performed using the quadrant method at each fraction.

2.2.3. Effect of initial concentration

A $K_2Cr_2O_7$ stock solution of 100 mg/L was used for achieving initial concentrations of Cr^{6+} between 10 to 100 mg/L. The non-magnetic sediment sample with grain size <0.5 mm was used. Four series of experiments were carried out, keeping constant the pH value at 4.5, 5.5, 6.5 and 7.5.

3. Results and discussion

3.1. Sediment chemistry and mineralogy

The grain size distribution curve (Fig. S1, Supplementary material) showed that the collected sediment is consisted of gravels at 25.8%, sand at 35.2% and clays at 5.0%. The serpentine origin of the tested sediments at all depths was confirmed by XRF and XRD analysis (Dermatas et al., 2015). The results of XRF analysis performed (Table 1) are consistent with previous bulk data. Fe and Cr concentrations did not vary substantially in the six particle size fractions analyzed, with the exception of higher concentrations of both elements observed in the fraction between 0.5 and 2 mm. Conversely, fractionation of the sediment on the basis of magnetic properties showed an accumulation of both Cr and Fe in the magnetic fraction of the sediment, which had double the Fe and 7× the Cr concentration compared to the non-magnetic fraction. The mass of the magnetic fraction weighed at 0.1 g per gram of bulk sediment. Based on this distribution, the mass balance for Fe between the non-magnetic and the magnetic sediment fractions closes with the measured Fe concentration in the bulk sample. Mg, Mn and Co showed slightly increased concentrations in the magnetic fraction as well, while Al and Si were significantly lower. These observations are related to the sediment minerals that prevail in the different fractions.

Fig. 1 presents the two XRD patterns of the bulk sediment sample and the magnetic fraction. Both patterns contain typical minerals of serpentine origin, including chromite/magnetite and chrysotile, as well as quartz and albite that are more representative of sediments with granitic background. The relative intensity of chromite and chrysotile is higher in the magnetic fraction XRD, while alumino-silicates are very low, which agrees with the accumulation of Fe and Cr in the magnetic fraction, and the lower concentration of Si.

The presence of chromite was verified by SEM-EDS analysis (Fig. 2). The results showed the occurrence of a spinel mainly covered by bulk serpentinized mass (black area). In addition chromite ($Fe^{2+}Cr_2O_4$) and Cr-magnetite ($Cr\text{-}Fe^{2+}F^{3+}{}_2O_4$) were also observed (Table S2, Supplementary material). The presence of chromite and magnetite with isomorphic substitutions between Mg with Fe^{2+} and Cr with Fe^{3+} is typical for serpentine soils and sediments (Barnes and Roeder, 2001; Farahat, 2008). Economou-Eliopoulos (2003) mentioned that apart from grained magnetite in a sediment matrix, magnetite can be associated with chromite since magnetite is the final product of sequential transformations to ferrian-chromite and finally to magnetite. Another option is the occurrence of magnetite as rims on chromite.

The mass balance for Fe, Al, Cr, Mg and Si calculated through quantitative XRD (Table S3, Supplementary material) and measured by XRF (Table 1) is shown in Table 2. The results indicate that the amorphous fraction consists of Fe, Mg and Si, while Al and Cr are accounted by their crystalline phases. Poorly crystallized goethite is likely the predominant amorphous iron hydroxide due to its common formation in serpentine soils (Chardot et al., 2007), without excluding the presence of other amorphous iron oxides. Amorphous Si oxides and cryptocrystalline or amorphous magnesite may also occur as alteration products of serpentinized ultramafic rocks (Peterson, 1984; Zachmann and Johannes, 1989).

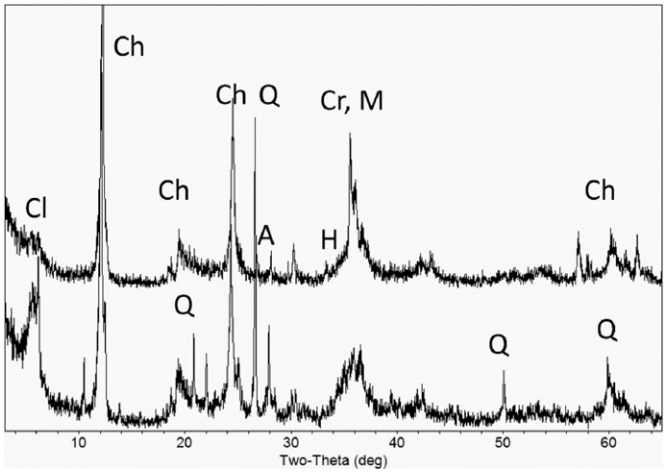

Fig. 1. Comparison of the XRD patterns of the bulk soil (bottom) and the magnetic fraction (top) (Ch: chrysotile, Cl: chlorite, Cr: chromite, M: magnetite, Q: quartz, A: albite, H: hematite).

Taking into account the PZC values (Table S4, Supplementary material) of the identified minerals, Cr^{6+} adsorption can mainly be attributed to several minerals that have high PZCs: Hematite (Singh et al., 1993) and amorphous goethite (Fendorf, 1995) that have been previously identified in serpentine soils in Greece (Kelepertzis et al., 2013) and in this study. In addition, chlorite (Brigatti et al., 2000) and magnetite (Jung et al., 2007) can contribute to Cr^{6+} removal via both reduction and adsorption. Chromite and chrysotile also have PZCs that can justify Cr^{6+} adsorption; however there is no information in the literature with respect of the sorption behavior of these minerals.

3.2. Batch experiments

3.2.1. Effect of pH and mineralogy

The effect of pH was first tested using the bulk sediment sample (Fig. 3a). The results showed a decreasing trend in Cr^{6+} removal with increasing pH. Maximum removal of almost 80% was achieved at pH 3. The desorption experiments indicated that removal of Cr^{6+} was not completely reversible, which in turn shows that two processes were responsible: adsorption, which is reversible and corresponds to the amount recovered at pH 11, and reduction, which is irreversible, and corresponds to the difference between removal and adsorption. It should be noted that throughout the experiments, oxidation Cr^{3+} to Cr^{6+} within the soil was deemed to be negligible, as indicated by batch oxidation experiments showing no appreciable Cr^{6+} within 24 h of leaching (unpublished data).

Table 1
Results of XRF analysis.

Soil sample	Grain size (mm)	Elements (mg/kg)							
		Fe	Al	Cr	Mg	Si	Mn	Co	Cr(VI)
1st fraction	d > 4.75	52,563	19,170	1724	152,220	226,240	830	117	n.q.
2nd fraction	2 < d < 4.75	64,323	13,511	3632	173,820	210,700	1032	156	n.q.
3rd fraction	0.5 < d < 2	67,179	12,515	4767	171,000	207,386	1092	162	n.q.
4th fraction	0.25 < d < 0.5	61,062	n.q.	2148	n.q.	n.q.	1175	n.q.	0,67
5th fraction	0.075 < d < 0.25	63,800	n.q.	1658	n.q.	n.q.	1248	n.q.	0,76
6th fraction	d < 0.075	69,786	n.q.	1522	n.q.	n.q.	1458	n.q.	0,81
"Bulk" soil	d < 0.5	68,523	17,354	3754	150,720	209,766	1215	153	1,47
"Non-magnetic" fraction	d < 0.5	61,278	12,281	2361	144,480	207,386	1164	149	0,87
"Magnetic" fraction	d < 0.5	129,290	3857	14,197	153,240	148,820	1264	263	0,94

n.q. not quantified.

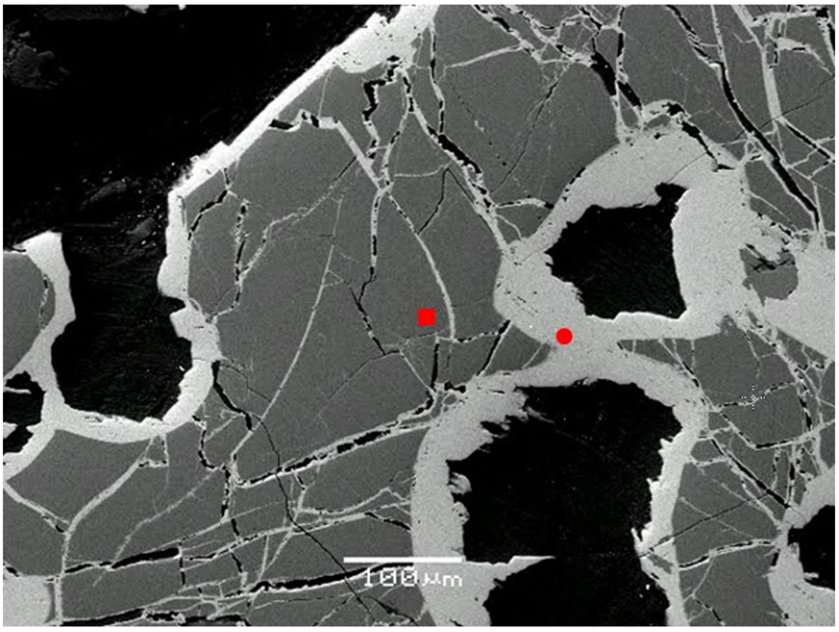

Fig. 2. SEM image of a soil sample with grain size <0.5 mm.

The relative contribution of adsorption and reduction was also a function of pH. The adsorption of Cr^{6+} was approximately constant and was determined as 50% of the removed Cr^{6+} in the pH range 4 to 7. The Cr^{6+} adsorption capacity in this pH range is calculated at 2 mg of Cr^{6+} per kilogram of sediment. At pH >7, adsorption decreased, but its relative contribution increased, reaching almost 100% of the removal. Conversely, reduction was more significant at pH 3 and 4, decreased to ~50% of removal in the pH range 5–7 and then decreased to almost zero at pH 7.5 and 8.5.

This inversely proportional trend of Cr^{6+} reduction with pH has also been observed in other studies investigating Cr^{6+} reduction in the geoenvironment (Henderson, 1994; Rai et al., 1988). Cr^{6+} reduction in the Vergina sediment is attributed to inorganic reductants such as Fe^{2+}, since very little organic matter (total organic carbon 0.08%, Table S1, Supplementary material) existed in the sample, and microbial reduction was prevented by sterilization. The identification of the magnetic fraction and Cr-magnetite in the SEM analysis also supports this notion.

In order to further explore the role of the magnetic fraction, two series of batch experiments were carried out, in which Cr^{6+} removal was tested in the non-magnetic (Fig. 3b) and magnetic (Fig. 3c) fractions. The non-magnetic fraction followed a similar trend of Cr^{6+} removal versus pH, but displayed an overall lower capacity for removal compared to the bulk sediment. Maximum removal at pH 3 was approximately 8 mg/kg or 60% of the total Cr^{6+}, significantly lower than the 80% achieved in the bulk sediment sample. The difference stems primarily from the lower reduction capacity, especially at pH > 4, while the contribution of adsorption was very similar, around 2 mg/kg for both the bulk and non-magnetic fractions. This indicates that the sorptive surfaces are similar in the bulk and in the non-magnetic fraction while the reducing compounds are depleted in the non-magnetic fraction.

Table 2
Mass balance for Fe, Al, Cr, Mg and Si concentrations as measured by XRF analysis and as determined via quantitative XRD.

	Fe (g/kg)	Al (g/kg)	Cr (g/kg)	Mg (g/kg)	Si (g/kg)
Total XRD	43,2	19,0	4,3	120,1	169,4
XRF	68,5	17,4	3,8	150,7	209,8
Amorphous (XRF-XRD)	25.3	−1.6	−0.5	30.6	40.4

The results of Cr^{6+} removal by the magnetic fraction confirmed the hypothesis that it has a high removal and reduction capacity. As observed from Fig. 3c, the maximum removal of Cr^{6+} by the magnetic fraction at pH 3 was higher than 90%. For pH values between 5 and 7, removal was measured at 50% (6.5 mg/kg) and is almost 1.5 times higher compared to the bulk sediment. The results also indicated that the adsorption contribution in the magnetic fraction was constant at 2 mg/kg. Thus, the increased removal was exclusively due to enhanced reduction.

Potential minerals with magnetic properties identified by XRD are primarily magnetite and to a lesser extent chromite. Kendelewicz et al. (1999) and He and Traina (2005), have reported that the reduction rate of Cr^{6+} by magnetite is relatively faster at acidic conditions than at neutral and alkaline pH values. Choi et al. (2008) observed that the reduction rate of Cr^{6+} decreased as the pH of the magnetite solution increased above the PZC of magnetite (~7.5), and the results obtained at equilibrium are qualitatively consistent with the results of this study. The mechanism for Cr^{6+} removal has been shown to be a combination of adsorption and reduction processes. The initial adsorption of Cr^{6+} on the surface of magnetite is followed by Cr^{6+} reduction on its reactive surface sites (Jung et al., 2007) with the percentage of Fe^{2+} on the surface of magnetite being a factor that controls the reduction of Cr^{6+} (Choi et al., 2008).

Comparing the adsorbed amount of Cr^{6+} by the bulk sample with the weighted average of the magnetic and non-magnetic fractions shows that the bulk sediment has almost equal adsorption capacity with the other two fractions. Regarding the removal capacity it is observed that the weighted sum of the two fractions is 10% higher than that of the bulk. A possible explanation is that the magnetite surface in the bulk sediment is likely not entirely available to react with the liquid phase as compared to isolating and suspending the magnetic fraction in solution with L:S of 50.

3.2.2. Effect of particle size

The effect of particle size at Cr^{6+} removal was tested in three fractions of the non-magnetic fraction: a) 0.25 mm < d < 0.5 mm, b) 0.075 mm < d < 0.25 mm and c) d < 0.075 mm. The magnetic fraction was removed in order to minimize reduction and isolate the adsorption process. As shown in Table 3, the mass of the magnetic fraction decreased with decreasing grain size. A possible explanation of this trend is that chromite and its alteration products including magnetite,

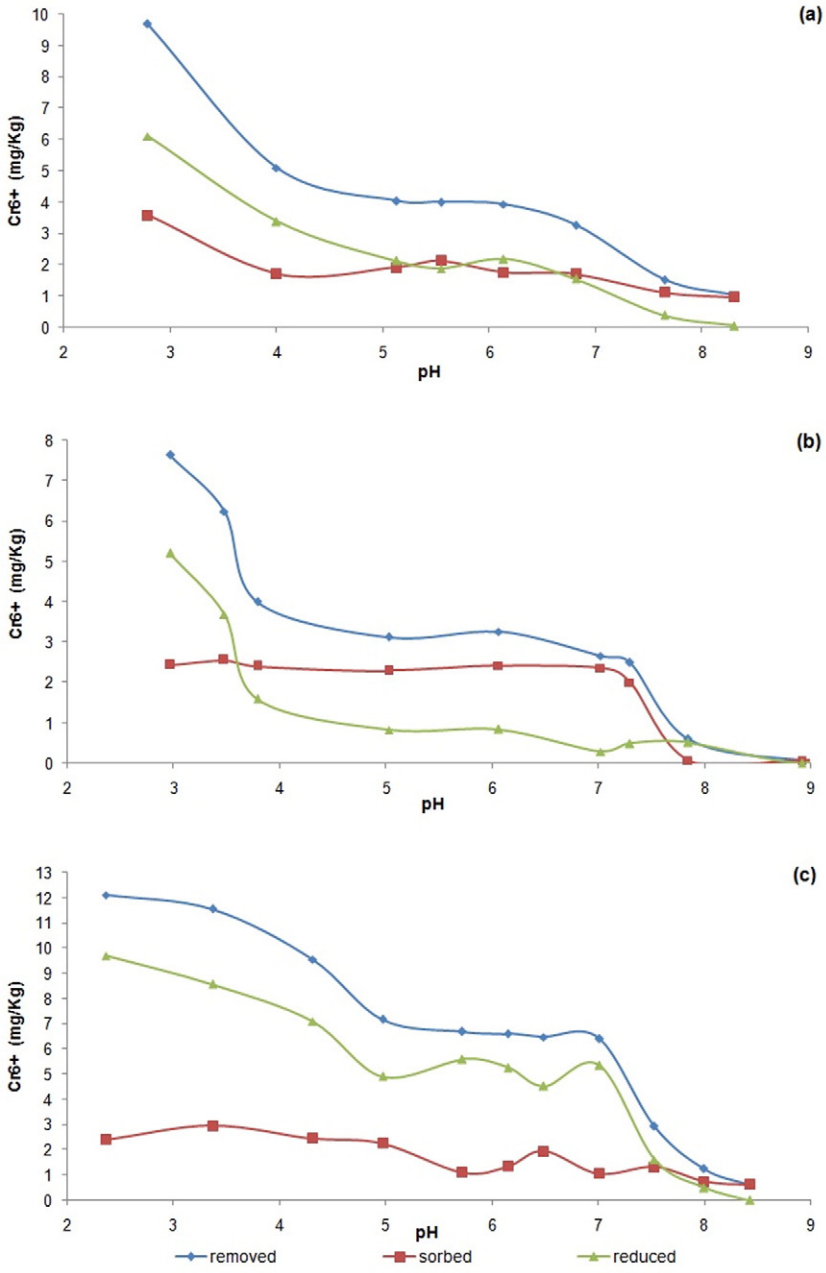

Fig. 3. Adsorption of Cr^{6+} ($[Cr^{6+}]_0 = 250$ μg/L) on a) the bulk soil, b) the non-magnetic fraction and c) the magnetic fraction (diamonds: removal; squares: adsorption; triangles: reduction).

which were observed in higher concentration in the magnetic fraction, belong to the group of spinels which exhibit resistance to weathering and accumulate in the coarser fraction.

The results of the batch tests (Fig. 4) showed that Cr^{6+} removal decreased with increasing particle size. The maximum removal at pH 3 decreased from 10 mg/kg in the <0.075 mm fraction to 8.5 mg/kg in the intermediate and 7.8 mg/kg in the 0.25 mm < d < 0.5 mm fraction. The weighted average of the three fractions is 8.5 mg/kg, while the measured maximum removal in the non-magnetic fraction at pH 3 was 7.6 mg/kg (Fig. 3b). Similar to the comparison of the bulk sediment with the individual magnetic and non-magnetic fractions, separating the sediment fractions increases removal efficiency.

Both the coarse and intermediate fractions exhibited zero reduction capacity at pH > 4, while the contribution of reduction at pH below 4 was approximately 50% of the total removal. At pH > 4, adsorption was the only mechanism for Cr^{6+} removal in the two coarser fractions and was approximately 2 mg/kg in the pH range 4.5–7.5, decreasing to almost zero at pH > 8. The finest fraction (<0.075 mm) maintained a similar adsorption capacity in the entire pH range, but had substantially higher reduction capacity at pH < 5, which increased linearly with decreasing pH.

Table 3
Properties of various particle size fractions.

Sample	SSA (m^2/g)	Fraction percentage	Mass of magnetic fraction per mass of "bulk" soil (g/g)
"Non-magnetic" fraction	55.95	100%	0.10
0.25 mm < d < 0.5 mm	45.84	44%	0.19
0.075 mm < d < 0.25 mm	52.49	36%	0.09
d < 0.075 mm	57.67	20%	0.02

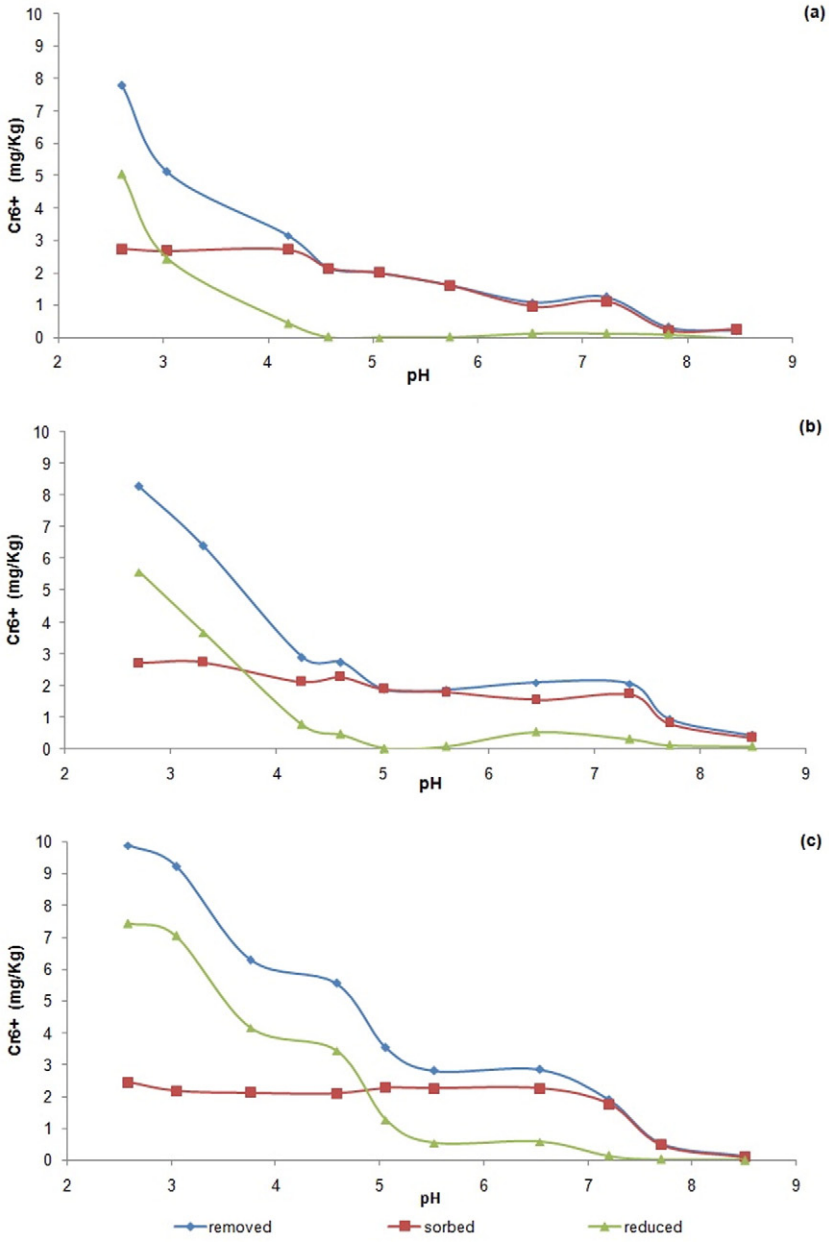

Fig. 4. Adsorption of Cr^{6+} ($[Cr^{6+}]_0 = 250$ μg/L) on a) the 0.25 mm < d < 0.5 mm soil fraction, b) the 0.075 mm < d < 0.25 mm soil fraction and c) the d < 0.075 mm soil fraction (diamonds: removal; squares: adsorption; triangles: reduction).

Both adsorption and reduction by magnetite are surface-driven processes, so that the specific surface area (SSA) is an important parameter to account for the observed differences between various fractions. In general, increasing the particle size the adsorption of metal ions decreases, since the larger particles are characterized by lower SSA values and thus have fewer active sites for adsorption per unit of mass of the adsorbent (Aravanakumar and Umar, 2011; Choudhury et al., 2014; Krishna and Swamy, 2012). Table 3 shows the BET-measured SSA values for the bulk non-magnetic fraction, as well as the individual size fractions. The determined SSA values are all very high, especially for the coarser fractions that should not include substantial vermiculite or chlorite that have high SSAs, indicating that the sediment fabric likely has substantial surface porosity. To put these values in perspective, typical pure goethite has SSA 25–90 m^2/g (Villalobos and Pérez-Gallegos, 2008), chlorite 25–150 m^2/g (Sparks, 2003), while quartz has SSA as low as 1–2 m^2/g (Meloni et al., 2012). Serpentine minerals generally have low SSAs, in the order of 7 m^2/g (Daval et al., 2013). Based on the observed mineralogical composition, it appears that all fractions have substantial surface porosity, which dominates the effect of particle size. This was further explored by normalizing reduction and adsorption using the measured SSA values.

Fig. 5 presents the molar mass of Cr^{6+} reduced and adsorbed per m^2 for the three particle size ranges, the weighted average of these and the non-magnetic fraction. In general, it can be observed that there are only small differences between the fraction for both reduction and adsorption. In terms of adsorption (Fig. 5a), the non-magnetic fraction shows identical behavior as the finer fraction a common phenomenon in soils and sediments. The coarser fractions show somewhat increased adsorption capacity at low pH values (pH 3 and 4) and decreased capacity at pH 6.5. SSA alone cannot explain these differences, as the adsorption increases with increased particle size, a counter-intuitive phenomenon. Differences in the slope of the adsorption curve are most likely related to the dominance of a different type of surface, i.e. to differences in the protonation behavior.

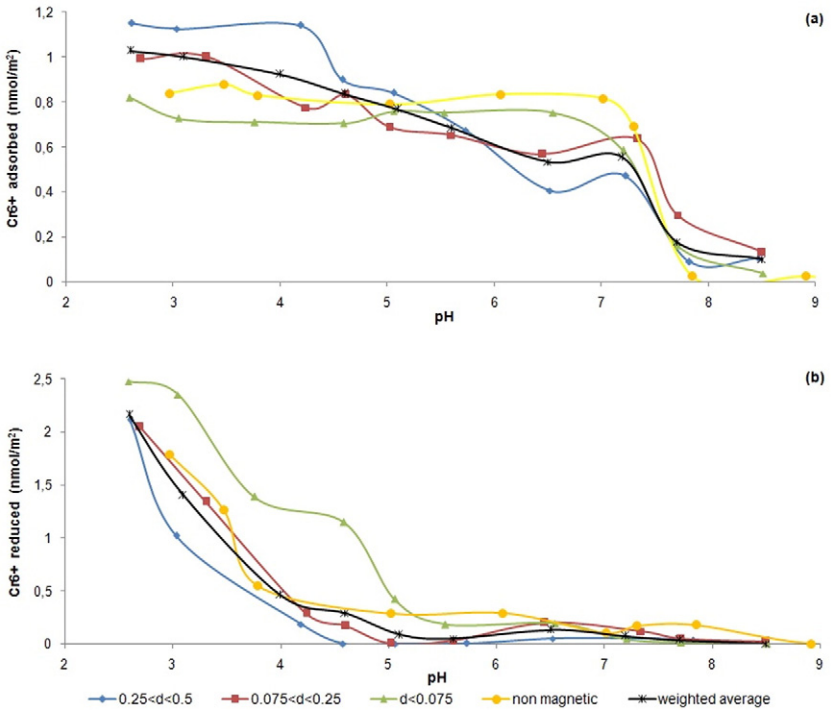

Fig. 5. Mass of Cr^{6+} adsorbed per m^2, for the three tested fractions and the non-magnetic fraction.

Adsorption on pure goethite reported by Villalobos and Pérez-Gallegos (2008) reached a maximum between 8 nmol/m^2 (SSA 70 m^2/g) and 10 nmol/m^2 (SSA 50 m^2/g) at pH 7, with a similar initial Cr^{6+} concentration of 5 μM (260 μg/L) and solid concentration (10 g/L). Assuming that all 25 g/kg of amorphous Fe (Table 2) are present as goethite, 40 g of goethite (α-FeOOH) would be present per kg of sediment, which in turn corresponds to an adsorption capacity of 0.4 nmol/m^2, making a simplifying assumption that goethite and the sediment have the same SSA of 50 m^2/g. The observed maximum capacity in the bulk non-magnetic fraction is 0.8 nmol/m^2, which indicates that there are additional sorption surfaces for Cr^{6+} in the amorphous iron fraction, which accounts for only 50% of the maximum adsorption. As previously discussed, hematite, chlorite and chrysotile are additional minerals with high PZC that may contribute to Cr^{6+} adsorption.

The reduction curve of the non-magnetic fraction follows more closely the intermediate fraction and the weighted average of all fractions. The finer fraction has a higher reduction potential and appears to play a more significant role at pH > 5, in which the bulk non-magnetic fraction maintains a small reduction capacity that is higher than the weighted average of the individual fractions. The effect of SSA for the reduction curves is overall straightforward, given that the reduction potential is increased with reduced particle size, as expected for a surface-driven phenomenon.

3.2.3. Effect of initial concentration

The effect of Cr^{6+} initial concentration on adsorption and reduction was tested on the non-magnetic fraction in the range of 10 to 100 mg/L Cr^{6+}, for four different pH values (4.5, 5.5, 6.5 and 7.5). The considerably higher concentrations used in this series were necessary in order to reach a plateau in the isotherms, while maintaining the L:S ratio identical as in the above batch experiments. As observed in Fig. 6, the sediment possesses substantially higher reductive and adsorptive capacity compared to the values measured in the non-magnetic fraction at initial concentration of 250 μg/L (Fig. 4b). This clearly demonstrates that the observed reduction is a surface-driven process, which requires partitioning of Cr^{6+} onto the solid phase in order for the reduction step to occur. In other words, reduction is partially driven by adsorption equilibria as well. This phenomenon has been previously discussed by Kendelewicz et al. (2000) and He and Traina (2005) for pure magnetite.

The reduction curves exhibit greater variability compared to the adsorption isotherms, especially at high Cr^{6+} initial concentrations. At pH 4.5, no plateau was reached and a reduction capacity of 900 mg/kg was measured at initial Cr^{6+} of 100 mg/L. At higher pH values, a plateau seemed to be reached in the range 400–500 mg/kg, however the variability at high concentrations was too high to make a reliable quantitative distinction between the different pH values. In general, it appears that at pH values above 5 the reduction is limited by the availability of H^+, which was also the case at the much lower initial Cr^{6+} concentration of 250 μg/L. For the reduction of 500 mg/kg (~1 mmol/kg) of Cr^{6+}, 3 mmol of Fe^{2+} are required stoichiometrically, or 3 mmol of pure magnetite according to the reaction (Peterson et al., 1997)

$$6Fe^{2+}Fe^{3+}O_4 + 2CrO_4^{2-} + 4H^+ \rightarrow 9\gamma Fe_2O_3 + 2CrOOH + H_2O$$

This corresponds to 168 mg of Fe^{2+} per kg sediment or 698 mg pure magnetite. Even though these experiments were conducted on the non-magnetic fraction, Fe^{2+} is present in Cr-magnetite, chromite, chlorite and other minerals in the matrix that cannot be isolated with simple magnetic separation. Given the higher percentages of these minerals in the sediment, this amount of available Fe^{2+} is clearly feasible.

The adsorption curves followed the trends of traditional isotherms, in which the increase in Cr^{6+} concentration leads to increase of Cr^{6+} adsorption up to 70 mg/L, above which it reaches a plateau for all pH values tested. This phenomenon is attributed to the saturation of the available surface sites. In addition, decrease of pH values causes increase in Cr^{6+} adsorption, for the same values of initial concentration. The decrease of pH from 7.5 to 4.5 doubled Cr^{6+} adsorption, from a maximum of 100 to 200 mg/kg, or approximately 25% of the total removal. The contribution of adsorption to removal was lower in this concentration range compared to the batch experiments with 250 μg/L initial concentration, in which it ranged between 35% at pH 3 and 95% at pH 8. The maximum adsorption capacity follows a logarithmic trend with pH (R^2 0.98) (Fig. S2, Supplementary material). This is explained by the

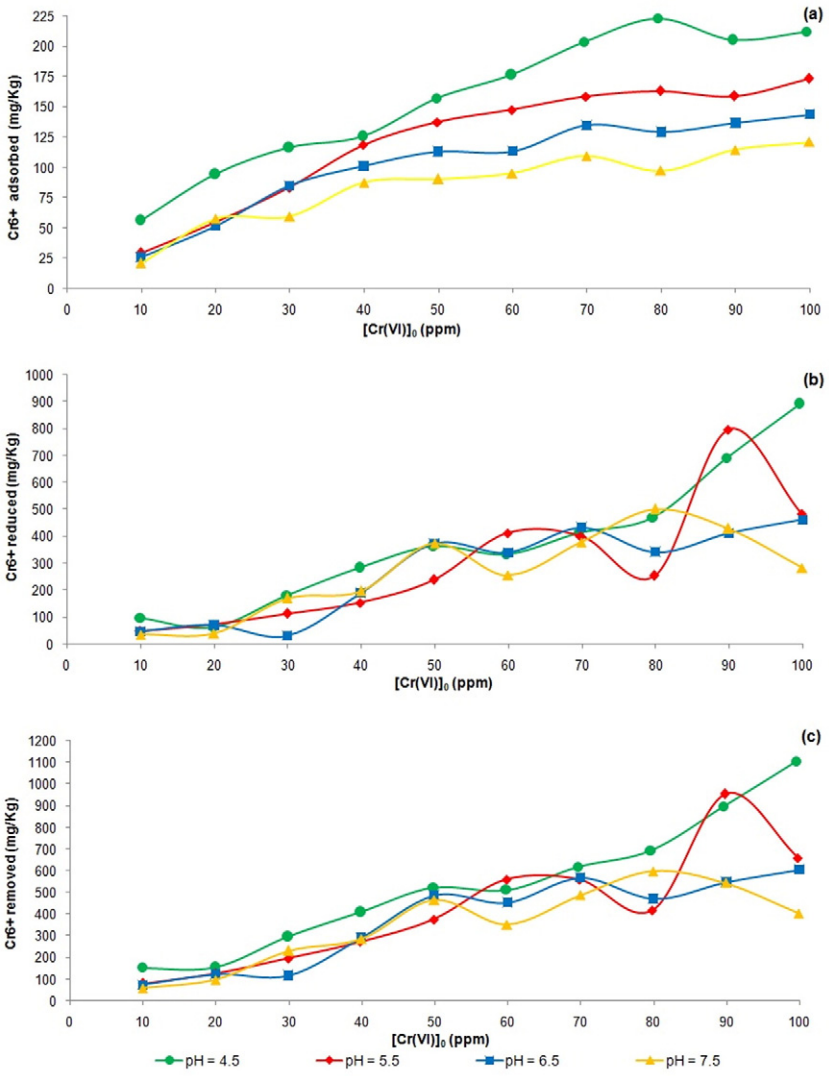

Fig. 6. Effect of Cr^{6+} initial concentration on (a) adsorption, (b) reduction and (c) total removal for four different pH values (4.5, 5.5, 6.5 and 7.5) at room temperature (25 °C).

increase in H^+, which increases positively charged surface sites and thus anion surface complexation (Sposito, 1989).

The adsorption and removal data presented in Fig. 6 were also used to fit Langmuir and Freundlich isotherms and to determine distribution factors that may be employed in transport modeling. While removal includes reduction, which is not traditionally modeled through isotherms, it is more practical to determine a single distribution factor to describe both processes, since they occur simultaneously. The linearized Langmuir (Eq. (2)) and Freundlich (Eq. (3)) isotherms and their associated constants are included in Table 4. At both equations C_e (mg/L) is the concentration of adsorbate remaining in the solution at equilibrium and q_e (mg/g) is the amount of adsorbate per unit mass of adsorbent.

$$\frac{C_e}{q_e} = \frac{1}{Q * b} + \frac{1}{Q} C_e \quad (2)$$

Where Q (mg/kg) is the maximum adsorption and b (L/mg) is the Langmuir bonding energy coefficient.

$$\log q_e = \log K + \frac{1}{n} \log C_e \quad (3)$$

Table 4
Langmuir and Freundlich constants for Cr(VI) adsorption and removal at four different pH values (4.5, 5.5, 6.5 and 7.5) at room temperature (25 °C).

pH	Langmuir						Freundlich					
	Adsorption			Removal			Adsorption			Removal		
	Q (mg/kg)	b (L/mg)	R^2	Q (mg/kg)	b (L/mg)	R^2	K (mg/kg)	n (L/mg)	R^2	K (mg/kg)	n (L/mg)	R^2
4.5	0.33	2.29E-03	0.94	6.07	8.11E-02	0.05	17.08	1.74	0.98	22.33	1.19	0.91
5.5	0.35	1.46E-03	0.85	33.00	2.83E-01	0.001	6.10	1.30	0.95	8.16	0.98	0.90
6.5	0.25	9.50E-04	0.91	0	0	0.001	6.58	1.42	0.93	7.62	1.00	0.87
7.5	0.19	6.26E-04	0.87	2.37	1.95E-02	0.08	6.28	1.50	0.90	7.62	1.01	0.87

Where K (mg/kg) and n (L/mg) are Freundlich parameters characteristic of the system, which are determined empirically and indicate the adsorption capacity and adsorption intensity, respectively. The higher the n factor, the more the expected heterogeneity of the available sorption sites.

The correlation coefficient (R^2) values (Table 4) indicate that the Freundlich isotherm describes better the experimental data in both cases (Figs. S3 and S4, Supplementary material), indicating the presence of heterogeneous surface sites on the solid surface. The K values were very close at pH above 5 for both adsorption and removal and increased substantially at pH 4.5. The natural pH of these sediments is between 7.5 and 8.5, so that acidic pH is unlikely to occur and the Kd values should not vary much in natural conditions. In addition, a n value >1 is indicative of the favorable nature of adsorption. The Langmuir isotherm could only describe the adsorption data and the slight difference between the R^2 factors for Freundlich and Langmuir isotherms indicates that the formation of a Cr^{6+} monolayer on the sediment surface is possible (Ajouyed et al., 2011; Vázquez et al., 2007).

4. Conclusions

This study focused on the sorption behavior of Cr^{6+} in serpentine sediments, a process that has not been studied despite the abundant literature in Cr^{6+} production in these geologic backgrounds. The results showed that both adsorption and reduction of Cr^{6+} take place and both increase as the pH decreased from 8.5 to 3. Reduction was most pronounced below pH 5, contributing 50% of the removal in the pH range 3–7. This process was associated with the presence of a magnetic fraction that includes magnetite and magnesio-chromite as primary minerals. Conversely, adsorption was constant in the pH range 3–7 and decreased sharply to reach zero at pH 8.5. This process is attributed to the presence of hematite and amorphous iron oxy-hydroxides in the sediment. Both processes are surface-driven with reduction being influenced by adsorption since partitioning of Cr^{6+} onto the solid surface is required before reduction takes place.

Evaluation of sorption as a function of particle size showed that the finer fraction (d < 0.075 mm) dominated the adsorption behavior of the sediment. However, coarser fractions were also found to possess substantial adsorption capacity, related to a high surface area, which is uncharacteristic of most coarse sediments. Thus, serpentine sediments are found to have substantial surface porosity even in coarser fractions.

Finally, Langmuir and Freundlich isotherms fit very well the experimental data, indicating thus the simultaneous heterogenity of the surface sites on the serpentinitic sediments and possibly the formation of a monolayer for Cr^{6+} adsorption. The resulting distribution factors may be used to describe Cr^{6+} retardation in transport models, either for removal (adsorption + reduction) or adsorption alone, by taking the respective datasets. Further research will focus on the development of surface complexation models that can describe Cr^{6+} adsorption on serpentine sediments, taking into account changes in groundwater chemistry.

Acknowledgements

This research was supported by the LIFE + CHARM project (LIFE10 ENV/GR/000601) and the Marie Curie project SPECHROM (No. 299392).

Appendix A. Supplementary material

Supplementary data to this article can be found online at http://dx.doi.org/10.1016/j.jconhyd.2016.12.009.

References

Abdel-Samad, H., Watson, P.R., 1997. An XPS study of the adsorption of chromate on goethite (a-FeOOH). Appl. Surf. Sci. 108, 371–377.
Adegoke, H.I., Adekola, F.A., 2012. Equilibrium sorption of hexavalent chromium from aqueous solution using synthetic hematite. Colloid J. 74, 420–426.
Ajouyed, O., Hurel, C., Ammari, M., Ben Allal, L., Marmier, N., 2010. Sorption of Cr(VI) onto natural iron and aluminum (oxy)hydroxides: effects of pH, ionic strength and initial concentration. J. Hazard. Mater. 174, 616–622.
Ajouyed, O., Hurel, C., Marmier, N., 2011. Evaluation of the adsorption of hexavalent chromium on kaolinite and illite. J. Environ. Protect. 2, 1347–1352.
Álvarez-Ayuso, E., García-Sánchez, A., Querol, X., 2007. Adsorption of Cr(VI) from synthetic solutions and electroplating wastewaters on amorphous aluminium oxide. J. Hazard. Mater. 142, 191–198.
Aravanakumar, K.S., Umar, A.K., 2011. Removal of hexavalent chromium from aqueous solution using *Vigna radiata* husk (green gram). Asian J. Chem. 23, 2635–2638.
Barnes, S.J., Roeder, P.L., 2001. The range of spinel compositions in terrestrial mafic and ultramafic rocks. J. Petrol. 42, 2279–2302.
Becquer, T., Quantin, C., Sicot, M., Boudot, J.P., 2003. Chromium availability in ultramafic soils from New Caledonia. Sci. Total Environ. 301, 251–261.
Bonifacio, E., Zanini, E., Boero, V., Franchini-Angela, M., 1997. Pedogenesis in a soil catena on serpentinite in north-western Italy. Geoderma 75, 33–51.
Brigatti, M.F., Franchini, G., Lugli, C., Medici, L., Poppi, L., Turci, E., 2000. Interaction between aqueous chromium solutions and layer silicates. Appl. Geochem. 15, 1307–1316.
Caillaud, J., Proust, D., Philippe, S., Fontaine, C., Fialin, M., 2009. Trace metals distribution from a serpentinite weathering at the scales of the weathering profile and its related weathering microsystems and clay minerals. Geoderma 149, 199–208.
Caillaud, J., Proust, D., Righi, D., Martin, F., 2004. Fe-rich clays in a weathering profile developed from serpentinite. Clay Clay Miner. 52, 779–791.
Chardot, V., Echevarria, G., Gury, M., Massoura, S., Morel, J.L., 2007. Nickel bioavailability in an ultramafic toposequence in the Vosges Mountains (France). Plant Soil 293, 7–21.
Cheng, C.H., Jien, S.H., Iizuka, Y., Tsai, H., Chang, Y.H., Hseu, Z.Y., 2011. Pedogenic chromium and nickel partitioning in serpentine soils along a toposequence. Pedology 75, 659–668.
Choi, J., Jung, Y., Lee, W., 2008. Fe(II)-initiated reduction of hexavalent chromium in heterogeneous iron oxide suspension. Kor. J. Chem. Eng. 25, 764–769.
Choudhury, T.R., Amin, M.N., Quraishi, S.B., Mustafa, A.I., 2014. Adsorption, desorption and kinetic study on hexavalent chromium removal from aqueous solution using groundnut shell. Res. J. Eng. Appl. Sci. 3, 1–6.
D'Amico, M., Julitta, F., Previtali, F., Cantelli, D., 2008. Podzolization over ophiolitic materials in the western Alps (Natural Park of Mont Avic, Aosta Valley, Italy). Geoderma 146, 129–137.
Daval, D., Hellmann, R., Martinez, I., Gangloff, S., Guyot, F., 2013. Lizardite serpentine dissolution kinetics as a function of pH and temperature including effects of elevated pCO_2. Chem. Geol. 351, 245–256.
Dermatas, D., Mpouras, T., Chrysochoou, M., Panagiotakis, I., Vatseris, C., Linardos, N., Theologou, E., Boboti, N., Xenidis, A., Papassiopi, N., Sakellariou, L., 2015. Origin and concentration profile of chromium in a Greek aquifer. J. Hazard. Mater. 281, 35–46.
Economou-Eliopoulos, M., 2003. Apatite and Mn, Zn, Co-enriched chromite in Ni-laterites of northern Greece and their genetic significance. J. Geochem. Explor. 80, 41–54.
Economou-Eliopoulos, M., Frei, R., Atsarou, C., 2014. Application of chromium stable isotopes to the evaluation of Cr(VI) contamination in groundwater and rock leachates from central Euboea and the Assopos basin (Greece). Catena 122, 216–228.
Fandeur, D., Juillot, F., Morin, G., Olivi, L., Cognigni, A., Ambrosi, J.P., Guyot, F., Fritsch, E., 2009. Synchrotron-based speciation of chromium in an Oxisol from New Caledonia: importance of secondary Fe-oxyhydroxides. Am. Mineral. 94, 710–719.
Fantoni, D., Brozzo, G., Canepa, M., Cipolli, F., Marini, L., Ottonello, G., Zuccolini, M.V., 2002. Natural hexavalent chromium in groundwaters interacting with ophiolitic rocks. Environ. Geol. 42, 871–882.
Farahat, E.S., 2008. Chrome-spinels in serpentinites and talc carbonates of the El Ideid-El Sodmein District, central eastern desert, Egypt: their metamorphism and petrogenetic implications. Chem. Erde 68, 193–205.
Fendorf, S.E., 1995. Surface reactions of chromium in soils and waters. Geoderma 67, 55–71.
Fernández-Pazos, M.T., Garrido-Rodriguez, B., Nóvoa-Muñoz, J.C., Arias-Estévez, M., Fernández-Sanjurjo, M.J., Núñez-Delgado, A., Álvarez, E., et al., 2013. Cr(VI) adsorption and desorption on soils and bio-sorbents. Water Air Soil Pollut. 224, 1366–1377.
Garnier, J., Quantin, C., Martins, E.S., Becquer, T., 2006. Solid speciation and availability of chromium in ultramafic soils from Niquelandia, Brazil. J. Geochem. Explor. 88, 206–209.
Gonzalez, A.R., Ndungu, K., Flegal, A.R., 2005. Natural occurrence of hexavalent chromium in the aromas red sands Aquifer, California. Environ. Sci. Technol. 39, 5505–5511.
He, Y.T., Traina, J.S., 2005. Cr(VI) reduction and immobilization by magnetite under alkaline pH conditions: the role of passivation. Environ. Sci. Technol. 39, 4499–4504.
Hejri, Z., Koohestanian, E., Reza Abedi, M., FarahBakhsh, I., 2015. The experimental study of the effect of hematite iron oxide (α–Fe_2O_3) nanostructure on reducing polluter's chromium and arsenic from aqueous solutions. J. Appl. Environ. Biol. Sci. 4, 38–46.
Henderson, T., 1994. Geochemical reduction of hexavalent chromium in the Trinity sand aquifer. Groundwater 32, 477–486.
Hseu, Z.Y., 2006. Concentration and distribution of chromium and nickel fractions along a serpentinitic toposequence. Soil Sci. 171, 341–353.
Jung, Y., Choi, J., Lee, W., 2007. Spectroscopic investigation of magnetite surface for the reduction of hexavalent chromium. Chemosphere 68, 1968–1975.
Kelepertzis, E., Galanos, E., Mitsis, I., 2013. Origin, mineral speciation and geochemical baseline mapping of Ni and Cr in agricultural topsoils of Thiva Valley (central Greece). J. Geochem. Explor. 125, 56–68.
Kendelewicz, T., Liu, P., Doyle, C.S., Brown Jr., G.E., 2000. Spectroscopic study of the reaction of aqueous Cr(VI) with Fe_3O_4 (111) surfaces. Surf. Sci. 469, 144–163.

Kendelewicz, T., Liu, P., Doyle, C.S., Brown Jr., G.E., Nelson, E.J., Chambers, S.A., 1999. X-ray absorption and photoemission study of the adsorption of aqueous Cr(VI) on single crystal hematite and magnetite surfaces. Surf. Sci. 424, 219–231.

Krishna, R.H., Swamy, A.V.V.S., 2012. Investigation on the effect of particle size and adsorption kinetics for the removal of Cr(VI) from the aqueous solutions using low cost sorbent. Eur. Chem. Bull. 7, 258–262.

Latsoudas, C., Sonis, C., 1991. Geological Map of Greece, Sheet Kolindros, Scale1:50,000. Institute of Geology and Mineral Exploration, Athens.

Margiotta, S., Mongelli, G., Summa, V., Paternoster, M., Fiore, S., 2012. Trace element distribution and Cr(VI) speciation in Ca–HCO_3 and Mg–HCO_3 spring waters from the northern sector of the Pollino massif, southern Italy. J. Geochem. Explor. 115, 1–12.

Meloni, P., Carcangiu, F., Delogu, F., 2012. Specific surface area and chemical reactivity of quartz powders during mechanical processing. Mater. Res. Bull. 47, 146–151.

Mills, C.T., Morrison, J.M., Goldhaber, M.B., Ellefsen, K.J., 2011. Chromium(VI) generation in vadose zone soils and alluvial sediments of the southwestern Sacramento Valley, California: a potential source of geogenic Cr(VI) to groundwater. Appl. Geochem. 26, 1488–1501.

Mishra, B., 2012. Adsorption of Hexavalent Chromium onto Goethite. National Institute of Technology Rourkela, Department of Mining Engineering.

Oliver, D.S., Brockman, F.J., Bowman, R.S., Kieft, T.L., 2003. Microbial reduction of hexavalent chromium under vadose zone conditions. J. Environ. Qual. 32, 317–324.

Otero, M., Cutillas-Barreiro, L., Nóvoa-Muñoz, J.C., Arias-Estévez, M., Fernández-Sanjurjo, M.J., Álvarez-Rodríguez, E., Núñez-Delgado, A., 2015. Cr(VI) adsorption/desorption on untreated and mussel shell-treated soil materials: fractionation and effects of pH and chromium concentration. Solid Earth 6, 372–383.

Oze, C., Bird, D.K., Fendorf, S., 2007. Genesis of hexavalent chromium from natural sources in soil and groundwater. PNAS 104, 6544–6549.

Oze, C., Fendorf, S., Bird, D.K., Robert, G., 2004. Chromium geochemistry of serpentine soils. Int. Geol. Rev. 46, 97–126.

Papanikolaou, D., 2009. Timing of tectonic emplacement of the ophiolites and terrane paleogeography in the Hellenides. Lithos 108, 262–280.

Peterson, J.A., 1984. Metallogenetic Maps Of The Ophiolite Belts Of The Western United States. USGS Miscellaneous Investigations Series Map Publications.

Peterson, M.L., White, A.F., Brown Jr., G.E., Parks, G.A., 1997. Surface passivation of magnetite by reaction with aqueous Cr(VI): XAFS and TEM results. Environ. Sci. Technol. 31, 1573–1576.

Peterson, M.L., Brown Jr., G.E., Parks, G.A., 1996. Direct XAFS evidence for heterogeneous redox reaction at the aqueous chromium/magnetite interface. Colloids Surf. A Physicochem. Eng. Asp. 107, 77–88.

Rai, D., Zachara, J.M., Eary, L.E., Ainsworth, C.C., Amonette, J.E., Cowan, C.E., Szelmeczka, R.W., Resch, C.T., Schmidt, R.L., Girvin, D.C., Smith, S.C., 1988. Chromium Reactions in Geologic Materials. Electric Power Research Institute, Palo Alto, California.

Richard, F.C., Bourg, A.C.M., 1991. Aqueous geochemistry of chromium: a review. Water Res. 25, 807–816.

Singh, D.B., Gupta, G.S., Prasad, G., Rupainwar, D.C., 1993. The use of hematite for chromium(VI) removal. J. Environ. Sci. Health A28, 1813–1826.

Sparks, D., 2003. Environmental Soil Chemistry. second ed. Academic Press.

Sposito, G., 1989. The Chemistry of Soils. Oxford University Press, Oxford, New York.

Tzou, Y.M., Wang, M.K., Loeppert, R.H., 2003. Sorption of phosphate and Cr(VI) by Fe(III) and Cr(III) hydroxides. Arch. Environ. Contam. Toxicol. 44, 445–453.

Vázquez, G., González-Álvarez, J., Garcia, A.I., Freire, M.S., Antorrena, G., 2007. Adsorption of phenol on formalde-hyde-pretreated *Pinus pinaster* bark: equilibrium and kinetics. Bioresour. Technol. 98, 1535–1540.

Villalobos, M., Pérez-Gallegos, A., 2008. Goethite surface reactivity: a macroscopic investigation unifying proton, chromate, carbonate, and lead(II) adsorption. J. Colloid Interface Sci. 2, 307–323.

WHO (World Health Organization), 1993. Guidelines for Drinking-Water Quality. second ed. (vol. 1-Recommendations, Geneva).

Xiao, W., Yang, X., He, Z., Li, T., 2014. Chromium-resistant bacteria promote the reduction of hexavalent chromium in soils. J. Environ. Qual. 43, 507–516.

Zachara, J.M., Girvin, D.C., Schmidt, R.L., Resch, C.T., 1987. Chromate adsorption on amorphous iron oxyhydroxide in presence of major groundwater ions. Environ. Sci. Technol. 21, 589–594.

Zachmann, D.W., Johannes, W., 1989. Cryptocrystalline magnesite. Monograph Series on Mineral Deposits. 28, pp. 15–28.